Oct 26th, 12:00 AM

Distortional Buckling Tests on Cold-formed Steel Beams

Cheng Yu

Benjamin W. Schafer

Seventeenth International Specialty Conference on Cold-Formed Steel Structures
Orlando, Florida, U.S.A November 4-5, 2004

Distortional Buckling Tests on Cold-Formed Steel Beams

Cheng Yu[1], Benjamin W. Schafer[2]

Abstract

Laterally braced cold-formed steel beams generally fail due to local or distortional buckling. When the compression flange is not restrained by attachment to sheathing or paneling, such as in negative bending of continuous members (joist, purlins, etc.), members are prone to distortional failures. However, distortional buckling remains a largely unaddressed problem in the main body of the North American Specification (NAS 2001). Only a limited amount of experimental data on unrestricted distortional buckling in bending is available, therefore a new series of distortional buckling tests was completed. The test details are selected specifically to insure that distortional buckling is free to form, but lateral buckling is restricted. Several design methods, including those of the U.S., Canada, Australia, and Europe as well as the Direct Strength Method are compared with the test results. Combined with our previously conducted local buckling tests (Yu and Schafer 2003), we can now provide experimental upper and lower bounds for the capacity of laterally braced cold-formed steel beams in common use in North America. Further, the experimental results have been investigated and extended through the use of non-linear finite element analysis with ABAQUS. This paper covers the setup of the distortional buckling tests, test results, finite element analysis and discussion of current design methods.

Introduction

Determination of the ultimate bending capacity of cold-formed steel C and Z members is complicated by yielding and the potential for local, distortional, and

1. Graduate Research Assistant, Johns Hopkins University, Baltimore, MD, 21228, USA. (cheng.yu@jhu.edu)
2. Assistant Professor, Johns Hopkins University, Baltimore, MD 21228, USA. (schafer@jhu.edu)

lateral-torsional buckling of the section, as shown in the finite strip analysis of Figure 1. Existing experimental and analytical work indicates that the current North American Specification provisions (NAS 2001) are inadequate for predicting bending capacity of C and Z members when distortional buckling occurs (e.g., Hancock et al. 1996, Rogers and Schuster 1995, Schafer and Peköz 1999, Yu and Schafer 2003). To investigate this problem, a two phase joint MBMA-AISI project was undergone at Johns Hopkins University. Phase 1 testing focused on the role of web slenderness in local buckling failures. A panel was through-fastened to the compression flange and a tight fastener spacing was selected to insure that distortional buckling and lateral-torsional buckling were restricted. The Phase 1 testing provided the upper-bound capacity for a bending member failing in the local mode and is summarized in Yu and Schafer (2003).

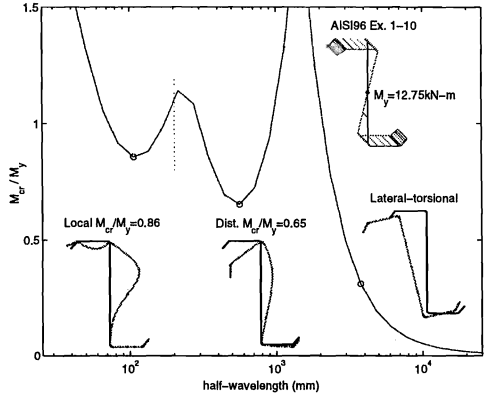

Figure 1 Buckling modes of a cold-formed steel beam

This paper details Phase 2 work on the distortional buckling of the same C and Z members previously examined in Phase 1. Although many C and Z members in bending have attachments (panel or otherwise) which stabilize the compression flange and help restrict distortional buckling, many do not. For example, negative bending of continuous members (joists, purlins, etc.) and wind suction on walls and panels (without interior sheathing) are common cases where no such beneficial attachments exist – these members are prone to distortional failures. Even when attachment to the compression flange exists it may not fully restrict distortional buckling, as may be the case for thin panels with large center-to-center fastener spacing and/or thick insulation between the purlin and panel. Flexural members are typically more prone to distortional failures than compression members, due to the dominance of local web buckling in typical compression members. Geometry unique to flexural members, such as the

sloping lip stiffener used in Zs is inefficient in retarding distortional buckling. For example, a typical 8 in. deep Z with t = 0.120 in. has a distortional buckling stress that is ½ the local buckling stress. The advent of higher strength steels also increases the potential for distortional failures (Schafer and Peköz 1999, Schafer 2002). In many braced flexural members, left unrestricted, distortional buckling is the expected failure mode.

Distortional Buckling Tests

Specimen Selection

The distortional buckling tests reported here employ nominally the same geometry as the previously conducted local buckling tests (Yu and Schafer 2003). Specimens were selected to provide systematic variation in web slenderness (h/t) while also varying the other non-dimensional parameters that govern the problem such as flange slenderness (b/t), edge stiffener slenderness (d/t) and relevant interactions, such as the web height to flange width (h/b) ratio. However, as commercially available sections were used, the manner in which the h/t variation could be completed was restricted by the availability of sections. A selection of the cross-sections selected for testing is summarized in Figure 2 and Table 1.

Geometry of the C and Z members used in the distortional buckling tests is summarized in Figure 3. The dimensions of the specimens were recorded at mid-length and mid-distance between the center and loading points, for a total of three measurement locations for each specimen. The mean dimensions, as determined from the three sets of measurements, are given in Table 2.

Table 1 Summary of specimens selected for testing

Performed Tests	No	h/t		b/t		d/t		h/b		d/b	
		min	max	min	max	min	max	min	max	min	max
Z Study 1: h, b, d fixed, t varied	7	71.3	138.2	21.9	39.3	7.0	13.4	3.2	3.6	0.28	0.37
Z Study 2: h, b, d fixed, t varied	2	126.6	140.4	38.6	42.0	10.1	11.5	3.2	3.3	0.26	0.28
C Study 1: h, b d fixed, t varied	6	80.7	238.6	20.3	59.1	6.4	20.3	3.8	4.1	0.26	0.35
C Study 2: b, d, t fixed, t varied	4	66.9	186.7	30.9	33.9	6.4	8.4	2.0	6.0	0.19	0.27
Total	19	66.9	238.6	20.3	59.1	6.4	20.3	2.0	6.0	0.19	0.37

Note: h – web depth; b – flange width; d – flange lip stiffener length; t – metal thickness.

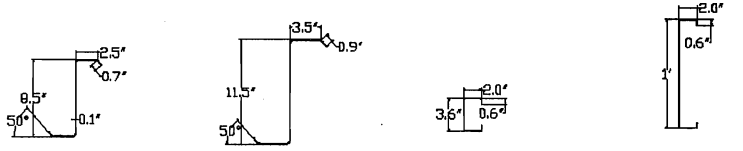

(a) 8.5 in. Z (b) 11.5 in. Z (c) Min depth C (d) Max depth C

Figure 2 Typical geometry of tested C and Z members

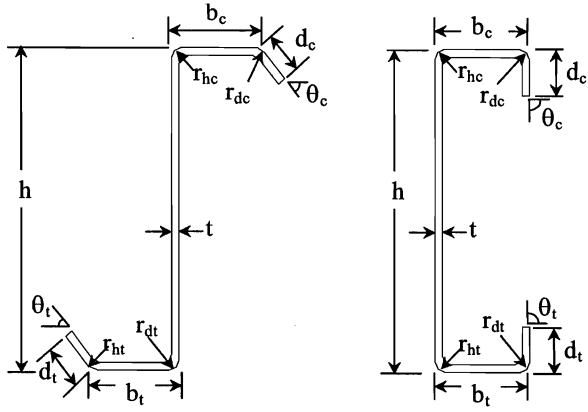

Figure 3 Definitions of specimen dimensions for Z and C

Table 2 Measured geometry of beams for distortional buckling tests

Test label	Specimen	h (in.)	b_c (in.)	d_c (in.)	θ_c (deg)	b_t (in.)	d_t (in.)	θ_t (deg)	r_{hc} (in.)	r_{dc} (in.)	r_{ht} (in.)	r_{dt} (in.)	t (in.)	f_y (ksi)	f_u (ksi)
D8.5Z120-4E1W	D8.5Z120-4	8.44	2.63	0.93	54.2	2.47	1.00	50.2	0.34	0.34	0.34	0.34	0.1181	61.35	83.11
	D8.5Z120-1	8.43	2.65	0.94	48.1	2.52	0.99	52.1	0.36	0.36	0.35	0.35	0.1181	61.89	83.27
D8.5Z115-1E2W	D8.5Z115-2	8.54	2.56	0.91	49.0	2.40	0.89	48.3	0.35	0.35	0.37	0.37	0.1171	64.14	83.88
	D8.5Z115-1	8.50	2.66	0.82	48.3	2.47	0.87	48.3	0.37	0.37	0.39	0.39	0.1166	65.79	84.67
D8.5Z092-3E1W	D8.5Z092-3	8.40	2.58	0.95	51.9	2.41	0.94	51.6	0.29	0.29	0.31	0.31	0.0893	57.59	72.13
	D8.5Z092-1	8.42	2.59	0.93	52.4	2.39	0.95	50.9	0.28	0.28	0.31	0.31	0.0897	57.75	72.58
D8.5Z082-4E3W	D8.5Z082-4	8.48	2.52	0.94	48.5	2.39	0.97	51.3	0.28	0.28	0.30	0.30	0.0810	59.21	74.02
	D8.5Z082-3	8.50	2.53	0.94	49.9	2.37	0.96	49.5	0.28	0.28	0.30	0.30	0.0810	58.99	73.85
D8.5Z065-7E6W	D8.5Z065-7	8.48	2.47	0.83	50.0	2.47	0.82	49.3	0.32	0.32	0.33	0.33	0.0642	62.36	83.47
	D8.5Z065-6	8.52	2.48	0.87	53.0	2.43	0.83	48.3	0.32	0.32	0.34	0.34	0.0645	63.34	83.37
D8.5Z065-4E5W	D8.5Z065-5	8.50	2.36	0.67	51.3	2.52	0.90	47.2	0.27	0.27	0.28	0.28	0.0645	62.79	83.24
	D8.5Z065-4	8.40	2.40	0.81	47.3	2.25	0.65	51.2	0.30	0.30	0.27	0.27	0.0619	58.26	78.45
D8.5Z059-6E5W	D8.5Z059-6	8.44	2.42	0.77	50.4	2.39	0.86	48.0	0.32	0.32	0.30	0.30	0.0618	58.54	79.11
	D8.5Z059-5	8.50	2.42	0.80	48.3	2.40	0.76	48.3	0.30	0.30	0.32	0.32	0.0615	59.05	79.40
D11.5Z092-3E4W	D11.5Z092-4	11.23	3.47	0.94	48.7	3.40	0.91	49.6	0.33	0.33	0.31	0.31	0.0887	69.89	89.91
	D11.5Z092-3	11.25	3.43	0.89	49.3	3.46	0.87	49.5	0.33	0.33	0.32	0.32	0.0889	70.11	90.25
D11.5Z082-3E4W	D11.5Z082-4	11.40	3.41	0.88	48.4	3.40	0.86	49.9	0.30	0.30	0.32	0.32	0.0812	73.65	93.21
	D11.5Z082-3	11.33	3.41	0.94	50.2	3.42	0.93	50.9	0.31	0.31	0.31	0.31	0.0818	71.80	92.02
D8C097-7E6W	D8C097-7	8.13	2.15	0.65	80.8	2.13	0.62	80.0	0.27	0.29	0.27	0.30	0.1001	85.18	90.77
	D8C097-6	8.15	2.09	0.64	81.0	2.09	0.61	80.0	0.27	0.29	0.27	0.30	0.1005	85.27	91.81
D8C097-5E4W	D8C097-5	8.06	2.00	0.66	86.7	1.99	0.67	83.0	0.28	0.30	0.28	0.28	0.0998	83.73	90.74
	D8C097-4	8.06	2.03	0.67	83.0	2.00	0.68	83.0	0.27	0.28	0.27	0.28	0.0998	84.16	91.07
D8C068-6E7W	D8C068-6	7.94	1.91	0.66	80.0	1.97	0.64	77.8	0.16	0.16	0.16	0.16	0.0708	78.94	80.87
	D8C068-7	7.94	1.97	0.64	76.5	1.95	0.67	77.5	0.16	0.16	0.16	0.16	0.0708	79.87	80.75
D8C054-7E6W	D8C054-7	8.01	2.04	0.53	83.4	2.03	0.57	88.7	0.24	0.23	0.21	0.23	0.0528	40.81	52.53
	D8C054-6	8.00	2.05	0.59	89.4	2.04	0.56	83.3	0.22	0.23	0.23	0.24	0.0520	40.68	50.86
D8C043-4E2W	D8C043-4	8.02	2.01	0.53	87.3	2.01	0.53	88.8	0.17	0.18	0.17	0.20	0.0459	45.44	61.04
	D8C043-2	8.03	1.99	0.52	88.9	1.98	0.54	87.7	0.18	0.19	0.20	0.19	0.0472	45.47	61.02
D8C033-1E2W	D8C033-2	8.15	1.99	0.68	87.1	1.91	0.63	85.8	0.17	0.30	0.20	0.30	0.0337	20.47	41.49
	D8C033-1	8.08	2.00	0.61	86.0	1.96	0.77	88.0	0.21	0.26	0.18	0.28	0.0339	20.35	42.19
D12C068-10E11W	D12C068-11	12.03	2.03	0.51	81.9	2.00	0.53	85.3	0.22	0.22	0.24	0.23	0.0645	32.90	56.92
	D12C068-10	12.05	2.02	0.54	85.8	1.98	0.51	94.8	0.24	0.24	0.27	0.23	0.0648	34.70	56.75
D12C068-1E2W	D12C068-2	11.92	2.05	0.52	82.5	2.03	0.59	77.4	0.26	0.24	0.25	0.24	0.0664	56.31	73.69
	D12C068-1	11.97	2.12	0.52	80.6	2.00	0.56	83.3	0.25	0.25	0.26	0.26	0.0668	55.86	73.61
D10C068-4E3W	D10C068-4	10.08	2.00	0.48	83.2	2.08	0.53	83.3	0.26	0.21	0.23	0.23	0.0626	22.01	40.26
	D10C068-3	10.10	2.07	0.53	80.7	2.08	0.52	81.9	0.24	0.23	0.23	0.22	0.0634	22.54	40.87
D3.62C054-3E4W	D3.62C054-4	3.73	1.88	0.41	87.0	1.87	0.43	89.0	0.26	0.24	0.27	0.27	0.0555	32.11	53.56
	D3.62C054-3	3.72	1.89	0.35	88.0	1.86	0.36	88.0	0.24	0.28	0.26	0.26	0.0556	32.91	53.32

Note: Typical specimen label is DxZ(or C)xxx-x. For example, D8.5Z120-1 means the specimen is 8.5 in. high for the web, Z- section, 0.12 in. thick and the beam number is 1. Typical test label is DxZ(or C)xxx-xExW. For example, test D8.5Z120-4E1W means the two-paired specimens are D8.5Z120-4 at the east side and D8.5Z120-1 at the west side.

Testing Setup

The basic testing setup is illustrated in Figure 4 and Figure 5. The 16 ft span length, four-point bending test, consists of a pair of 18 ft long C or Z beams in parallel loaded at the 1/3 points. The members are oriented in an opposed fashion, such that in-plane rotation of the C or Z leads to tension in the panel, and thus provides additional restriction against lateral-torsional buckling. Small angles, 1.25 × 1.25 × 0.057 in., are attached to the tension flanges every 12 in. Hot-rolled tube sections, 10 × 7.5 × 6 × 0.25 in., bolt the pair of C or Z beams together at the load points and the supports, and help insure shear and web crippling problems are avoided at these locations.

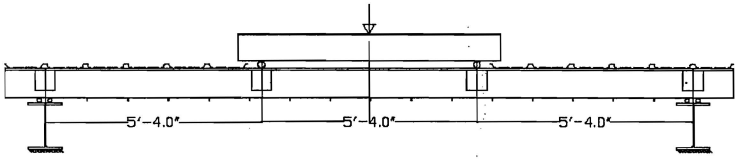

Figure 4 Elevation view of distortional buckling tests

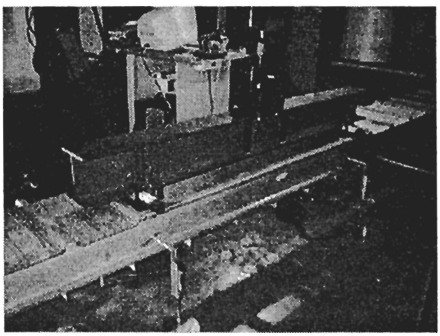

Figure 5 Panel setup for distortional buckling tests

No panel is placed inside the constant moment region (Figure 5). Instead, the through-fastened panel, t = 0.019 in., 1.25 in. high rib, is attached to the compression flanges in the shear spans only to restrict both the distortional and the lateral-torsional buckling in these regions, but leave distortional buckling free to form in the midspan. The loading system employs a 20 kip MTS actuator, which has a maximum 6 in. stroke. The test was performed in displacement control at a rate of 0.0015 in./sec. An MTS 407 controller and load cell monitored the force and insured the desired displacement control was met. Meanwhile, specimen deflections were measured at the 1/3 points with position transducers.

Panel-to-Purlin Fastener Configuration

The panel-to-purlin fastener configuration employed in the distortional buckling tests is the same as that used in the earlier local buckling tests, except the through-fastened panel in the constant moment region is removed. This setup is expected to restrict later-torsional buckling while allowing distortional and local buckling to occur. Examination of the ratio of the elastic distortional buckling moment (M_{crD}) to elastic local buckling moment (M_{crL}) indicates that a large number of members, particularly the Zs, are anticipated to fail in a mechanism dominated by distortional buckling (i.e., $M_{crD}/M_{crL} \leq 1$). Even when $M_{crD}/M_{crL} > 1$ distortional buckling may govern because of reduced post-buckling strength in distortional failures (Schafer and Peköz 1999).

Table 3 Elastic buckling loads of performed tests

Test label	M_y (kips-in.)	$M_{crL\text{-}FS}/M_y$	$M_{crD\text{-}FS}/M_y$	$M_{crL\text{-}FE}/M_y$	$M_{crD\text{-}FE}/M_y$	$M_{crLTB\text{-}FE}/M_y$
D8.5Z120-4E1W	534	2.76	1.41	2.85	1.45	2.28
D8.5Z115-1E2W	548	2.56	1.27	>2.65	1.31	2.14
D8.5Z092-3E1W	374	1.75	1.12	1.83	1.20	2.00
D8.5Z082-4E3W	352	1.36	0.93	1.42	1.00	>1.61
D8.5Z065-7E6W	295	0.81	0.67	0.86	0.72	>1.02
D8.5Z059-6E5W	259	0.80	0.65	0.84	0.71	>0.98
D11.5Z092-3E4W	806	0.76	0.52	0.79	0.58	>0.94
D11.5Z082-3E4W	780	0.60	0.45	0.64	0.49	>0.78
D8C097-5E4W	473	1.61	1.25	1.68	1.29	1.13
D8C068-6E7W	319	0.87	0.86	0.92	0.88	>1.06
D8C054-7E6W	122	0.93	1.06	0.96	1.06	>1.18
D8C043-4E2W	121	0.64	0.80	0.71	>0.88	>0.88
D8C033-1E2W	40	0.78	1.53	0.83	>1.05	>1.05
D10C068-4E3W	110	1.55	1.65	1.67	1.69	>2.06
D12C068-1E2W	219	0.78	0.84	0.92	0.95	>1.17
D3.62C054-3E4W	33	4.18	2.00	>3.64	2.00	2.85

Note: lower bounds are given to those buckling modes which are not included in the first 30 eigenmodes calculated in the ABAQUS analysis.

The elastic buckling loads of all performed tests are summarized in Table 3 where $M_{crL\text{-}FS}$ and $M_{crD\text{-}FS}$ respectively is the summation of local and distortional buckling moments for the two specimens in each test (calculated by the finite strip software CUSFM). $M_{crL\text{-}FE}$, $M_{crD\text{-}FE}$ and $M_{crLTB\text{-}FE}$ respectively is the elastic local, distortional and lateral-torsional buckling loads calculated by finite element software ABAQUS considering the complete testing setup (further details of the ABAQUS modeled are provided after the test results). M_y is the summation of the yield moments of both specimens in each test. As shown in Table 3, all tests except D8C097-5E4W have either local ($M_{crL\text{-}FE}$) or distortional

buckling ($M_{crD\text{-}FE}$) to be the first buckling mode and later-torsional buckling ($M_{crLTB\text{-}FE}$) is successfully restricted. Further, the test setup does not change the local and distortional buckling moments significantly (compare CUFSM vs. ABAQUS results to observe this). Distortional buckling is expected to be the initial failure mechanism for all Z beams and local or distortional for the C beams.

Tension Tests

Tension tests were carried out following "ASTM E8–00 Standard Test Methods for Tension Testing of Metallic Material" (ASTM, 2000). Three tensile coupons were taken from the end of each specimen: one from the web flat, the other two from top and bottom flanges. An MTS 634.11E-54 extensometer was employed to monitor the deformation. Test results are summarized in Table 2. It is shown that all the Z beams have similar material properties; the yield stresses are between 60 to 70 ksi and the f_u/f_y ratios are around 130%. On the contrary, the C beams have greatly varying material properties, the yield stresses are measured from 20 to 85 ksi, and the f_u/f_y ratios is from the lowest 101% (for a high strength material) to the highest 207% (for a low strength material). The tested yield stresses are employed to calculate the beam strength in all cases. The elastic moduli E is assumed to be 29500 ksi in all of the members. This E value is supported by tension test results during Phase 1 experiments.

Table 4 Distortional buckling test results

Test label	Specimen	M_y (kips-in.)	M_{test} /M_y	$M_{cr\ell}$ /M_y	M_{crd} /M_y	M_{test}/ M_{AISI}	M_{test}/ M_{S136}	M_{test}/ M_{NAS}	M_{test}/ M_{AN}	M_{test}/ M_{EN}	M_{test}/ $M_{DS\ell}$	M_{test}/ M_{DSd}
D8.5Z120-4E1W	D8.5Z120-4*	265	0.96	2.77	1.48	0.95	0.95	0.95	1.08	1.00	0.96	1.08
	D8.5Z120-1	269	0.94	2.75	1.35	0.93	0.93	0.93	1.09	1.00	0.94	1.09
D8.5Z115-1E2W	D8.5Z115-2	271	0.88	2.63	1.34	0.86	0.86	0.86	1.02	0.92	0.88	1.02
	D8.5Z115-1*	278	0.85	2.49	1.19	0.88	0.88	0.88	1.03	0.93	0.85	1.03
D8.5Z092-3E1W	D8.5Z092-3*	186	0.82	1.75	1.12	0.83	0.85	0.82	1.01	0.88	0.82	1.01
	D8.5Z092-1	188	0.82	1.74	1.12	0.83	0.85	0.83	1.00	0.87	0.82	1.00
D8.5Z082-4E3W	D8.5Z082-4*	176	0.72	1.36	0.93	0.77	0.81	0.76	0.95	0.83	0.77	0.95
	D8.5Z082-3	176	0.72	1.36	0.94	0.77	0.81	0.76	0.94	0.83	0.77	0.94
D8.5Z065-7E6W	D8.5Z065-7*	146	0.64	0.81	0.65	0.75	0.82	0.75	0.96	0.93	0.81	0.96
	D8.5Z065-6	149	0.63	0.81	0.69	0.72	0.79	0.72	0.92	0.88	0.79	0.92
D8.5Z065-4E5W	D8.5Z065-5	144	0.56	0.76	0.61	0.70	0.75	0.70	0.86	0.83	0.72	0.86
	D8.5Z065-4*	122	0.65	0.88	0.68	0.72	0.80	0.72	0.97	0.90	0.80	0.97
D8.5Z059-6E5W	D8.5Z059-6*	129	0.55	0.80	0.66	0.65	0.71	0.65	0.83	0.80	0.70	0.83
	D8.5Z059-5	130	0.55	0.79	0.64	0.64	0.70	0.64	0.83	0.79	0.69	0.83
D11.5Z092-3E4W	D11.5Z092-4	402	0.65	0.76	0.52	0.85	0.92	0.85	1.07	1.15	0.84	1.07
	D11.5Z092-3*	404	0.65	0.75	0.51	0.86	0.93	0.86	1.07	1.07	0.84	1.07
D11.5Z082-3E4W	D11.5Z082-4*	393	0.59	0.59	0.43	0.86	0.91	0.86	1.06	1.03	0.84	1.06
	D11.5Z082-3	387	0.60	0.61	0.47	0.84	0.89	0.84	1.03	1.02	0.84	1.03
D8C097-7E6W	D8C097-7	251	0.81	1.57	1.14	0.85	0.88	0.85	0.99	0.90	0.83	0.99
	D8C097-6*	250	0.82	1.57	1.16	0.85	0.89	0.85	0.99	0.91	0.83	0.99
D8C097-5E4W	D8C097-5*	234	0.71	1.61	1.26	0.73	0.76	0.76	0.84	0.77	0.71	0.84
	D8C097-4	238	0.69	1.61	1.25	0.72	0.74	0.72	0.83	0.75	0.70	0.83
D8C068-6E7W	D8C068-6	158	0.67	0.87	0.88	0.76	0.85	0.83	0.89	0.84	0.82	0.89
	D8C068-7*	161	0.65	0.87	0.83	0.77	0.86	0.84	0.89	0.85	0.80	0.89
D8C054-7E6W	D8C054-7	61	0.79	0.95	1.02	0.86	0.96	0.85	1.01	0.98	0.95	1.01
	D8C054-6*	60	0.80	0.93	1.12	0.86	0.95	0.85	1.00	0.98	0.97	0.99
D8C043-4E2W	D8C043-4*	60	0.72	0.63	0.78	0.90	0.97	0.90	1.00	1.03	0.99	1.01
	D8C043-2	61	0.70	0.66	0.80	0.86	0.94	0.94	0.98	0.98	0.95	0.97
D8C033-1E2W	D8C033-2	20	0.82	0.75	1.60	0.82	0.91	0.90	0.90	0.97	1.05	0.89
	D8C033-1*	20	0.81	0.75	1.45	0.82	0.91	0.91	0.93	1.00	1.04	0.92
D12C068-10E11W	D12C068-11*	107	0.88	0.79	0.84	0.92	1.05	1.05	1.21	1.13	1.12	1.21
	D12C068-10	112	0.84	0.77	0.84	0.88	1.00	1.00	1.15	1.07	1.08	1.15
D12C068-1E2W	D12C068-2*	188	0.52	0.49	0.52	0.67	0.72	0.70	0.86	0.79	0.79	0.86
	D12C068-1	188	0.52	0.51	0.54	0.67	0.72	0.70	0.85	0.78	0.77	0.85
D10C068-4E3W	D10C068-4*	53	0.95	1.55	1.60	0.95	1.01	1.01	1.05	1.01	0.98	1.05
	D10C068-3	57	0.90	1.56	1.68	0.90	0.94	0.95	0.96	0.94	0.91	0.97
D3.62C054-3E4W	D3.62C054-4	16	1.04	4.38	2.19	1.08	1.08	1.08	1.07	1.08	1.04	1.05
	D3.62C054-3*	16	1.04	4.31	1.88	1.14	1.14	1.11	1.12	1.10	1.04	1.09

Note *: Controlling specimen, weaker capacity by AISI (1996)

Distortional Buckling Test Results

Summaries of the distortional buckling test results are given in Table 4. Included for each test are the elastic buckling moments ($M_{cr\ell}$, M_{crd}) as determined by the finite strip method using CUFSM (Schafer 2001) and the ratios of test-to-predicted capacities for several design methods including the existing American Specification, M_{AISI} (AISI 1996), the existing Canadian Standard, M_{S136} (S136 1994), the newly adopted North American Specification, M_{NAS} (NAS 2001), the existing Australia/New Zealand Standard, M_{AN} (AS/NZS 1996), the existing European Standard EN1993, M_{EN} (EN1993 2002) and the recently proposed Direct Strength Method (DSM, Schafer and Peköz, 1998a; Schafer, 2002 – $M_{DS\ell}$ for local failure M_{DSd} for distortional failures).

The actuator load-displacement responses of all the distortional buckling tests are given in Figure 6 to Figure 9. Compared with the Phase 1 local buckling tests, more non-linear response is observed prior to formation of the failure mechanism. The specimens which have a capacity at or near the yield moment ($M_{test}/M_y \sim 1$, see Table 4) exhibit the most nonlinear deformation prior to failure; while the more slender specimens have essentially elastic response prior to formation of a sudden failure mechanism.

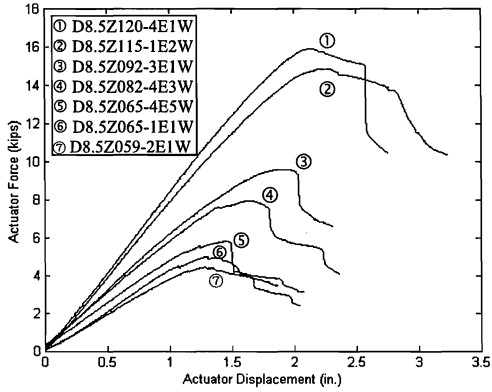

Figure 6 Actuator force-displacement responses of distortional buckling tests - Group 1

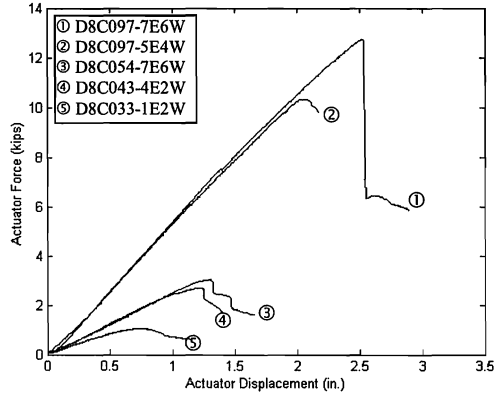

Figure 7 Actuator force-displacement responses of distortional buckling tests - Group 2

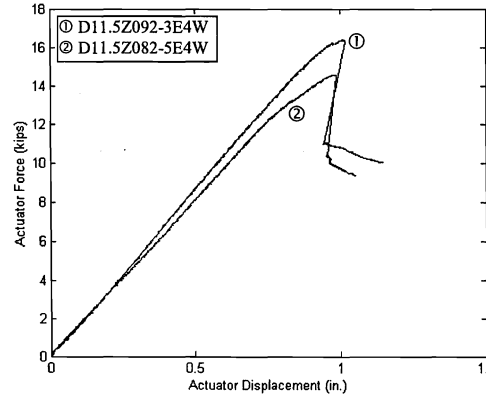

Figure 8 Actuator force-displacement responses of distortional buckling tests - Group 3

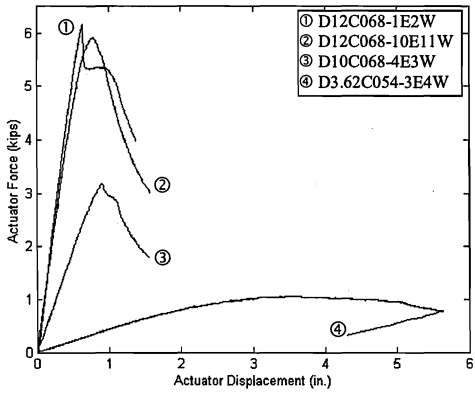

Figure 9 Actuator force-displacement responses of distortional buckling tests - Group 4

Comparison with Local Buckling Tests

For the Z beams Figure 10 provides a typical comparison between the local buckling and distortional buckling tests. The buckling wavelength is visibly longer in the distortional buckling test and the compression flange rotates about the web/compression flange juncture. This is expected as the Z beams have an elastic distortional buckling moment (M_{crd}) which is lower than local buckling for all the tests. Some of the C beams exhibited similar behavior, but in general the response of the C beams is more complicated. All of the C beams were observed to buckle at longer wavelengths than in the local buckling tests. Typically, the compression flanges of the C beams did not exhibit the same large rotations as observed in the Z beams. In the post-buckling range the majority of C beams include some rotation of compression flange, but in many cases translation and rotation of the cross-section as well. This observation indicates a more complicated collapse response and the possible interaction of distortional buckling with local/lateral-torsional buckling in the C beams.

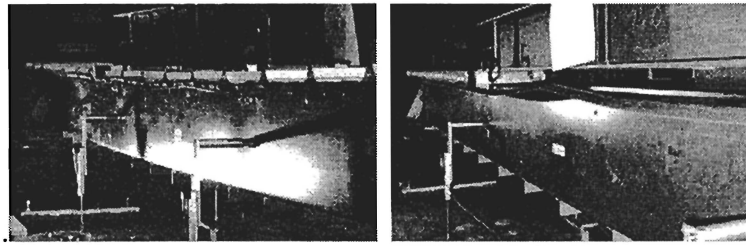

(a) Local buckling test 11.5Z092-1E2W (b) Distortional buckling test D11.5Z092-3E4W

Figure 10 Comparison of tests on 11.5Z092

Among 25 local buckling tests (Yu and Schafer 2003) and 19 distortional buckling tests, 9 pairs of tests use beams with nominally identical geometry and material. The test comparison for these specimens is summarized in Table 5. The notations of P_y, P_{crL}, P_{crD} are respectively the actuator load, P, that causes yielding, elastic local buckling, or elastic distortional buckling in the beam. On average, the beam bending strength will lose 17% when the through-fastened panel is removed from the compression flanges. The experimental results between the Phase 1 local buckling tests and the Phase 2 distortional buckling tests reported here indicate that the two tests in each pair have the same elastic stiffness, but different peak loads and buckling and post-buckling behavior. Typical comparisons of the actuator force vs. displacement response is shown in Figure 11. The distortional buckling tests present more nonlinear behavior before failure than the local buckling tests. However, larger deformations were observed in the web for the local buckling tests. For the distortional buckling tests, the failure in the compression flange is dominant, but lateral-torsional buckling is also involved in post-buckling region for some distortional buckling tests. It can be seen that with the through-fastened panel removed, the cold-formed steel C and Z beams have lower bending strength and less flexibility (less out-of-plane deflection before buckling) as expected.

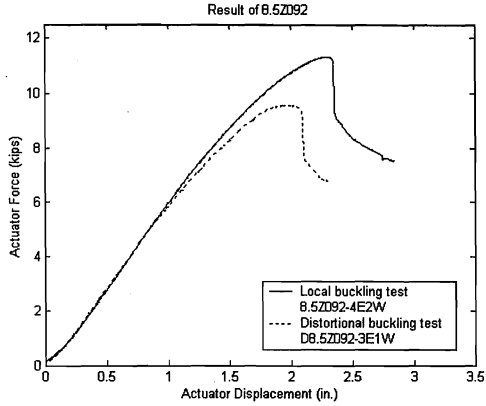

(a) 8.5 in. deep Z beams with nominal t=0.092 in.

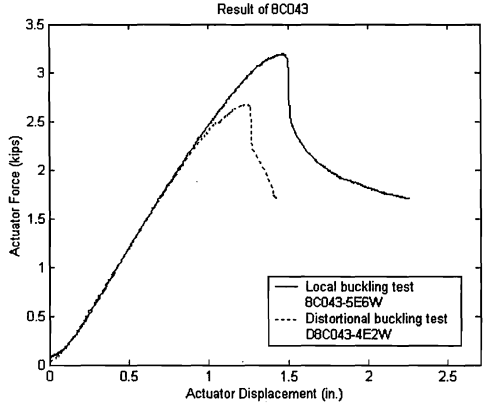

(b) 8 in. deep C beams with nominal t=0.043 in.

Figure 11 Comparison of local and distortional buckling tests

Table 5 Comparison of 9 pairs of identical tests

Pair No.	Local buckling test label	Distortional buckling test label	P_L (kip)	P_D (kip)	P_D/P_L
1	8.5Z120-3E2W	D8.5Z120-4E1W	17520	15870	91%
2	8.5Z092-4E2W	D8.5Z092-3E1W	11330	9566	84%
3	8.5Z082-1E2W	D8.5Z082-4E3W	10130	7921	78%
4	8.5Z059-2E1W	D8.5Z059-4E3W	6180	4439	72%
5	8C054-1E8W	D8C054-7E6W	3492	3032	87%
6	8C043-5E6W	D8C043-4E2W	3195	2678	84%
7	12C068-3E4W	D12C068-1E2W	8542	6160	72%
8	12C068-9E5W	D12C068-10E11W	6505	5912	91%
9	3.62C054-1E2W	D3.62C054-3E4W	1263	1071	85%
				Average	83%

Note: P_L --- actuator peak load of the local buckling test
P_D --- actuator peak load of the distortional buckling test

Comparison with Design Methods

Six design methods are considered for comparison: AISI (1996), S136 (1994), AS/NZS (1996), NAS (2001), EN1993 (2002) and DSM (2003). Specific specification predictions of the tested beams are listed in Table 4. Table 6 provides a summary of the test-to-predicted ratios. On average, all six methods give good strength predictions for the local buckling tests. The Direct Strength Method (DSM) uses a single strength curve, while the other five methods apply effective width concepts in the calculation of bending strength. For distortional buckling, only AS/NZS, EN1993 and DSM have specific methodologies. AS/NZS and DSM employ the minimum of separate local and distortional buckling strength predictions, while EN1993 assumes distortional buckling is an additional reduction on top of local buckling. Table 6 shows that all three methods provide reasonable strength predictions for the tests, though Eurocode still remains about 5% unconservative on average. The Australian/New Zealand code and Direct Strength Method's employ the same basic procedure and are quite similar for the distortional buckling tests. DSM statistically gives the best results for any of the distortional buckling methods. While, AISI, S136 and NAS provide systematically unconservative predictions for the distortional buckling strength, with an average error between 10~15%. AISI (1996), S136 (1994) and NAS (2001) are only applicable to local buckling failures. Figure 12 provides a graphical comparison of the NAS predictions for both series of tests.

Table 6 Summary of test-to-predicted ratios

			M_{test}/M_{AISI}	M_{test}/M_{S136}	M_{test}/M_{NAS}	M_{test}/M_{AN}	M_{test}/M_{EN}	M_{test}/M_{DSM}
Local buckling tests	Controlling specimens	μ	1.01	1.06	1.02	1.01	1.01	1.03
		σ	0.04	0.04	0.05	0.04	0.06	0.06
	Second specimens	μ	1.00	1.05	1.01	1.00	1.01	1.03
		σ	0.05	0.06	0.07	0.05	0.06	0.07
Dist. buckling tests	Controlling specimens	μ	0.85	0.91	0.87	1.02	0.96	1.01
		σ	0.11	0.10	0.11	0.09	0.10	0.08
	Second specimens	μ	0.83	0.88	0.85	0.99	0.95	0.99
		σ	0.10	0.10	0.11	0.09	0.11	0.09

Note: μ – average; σ – standard deviation

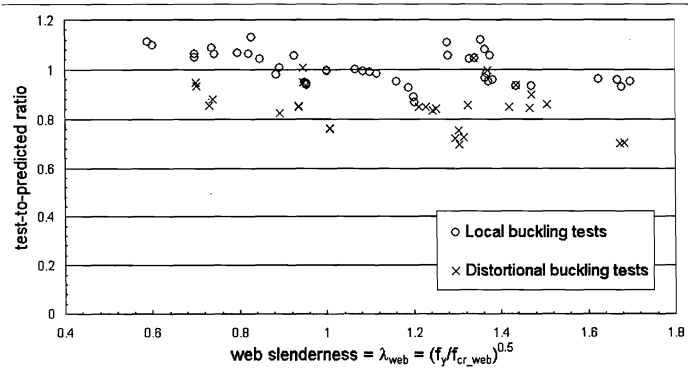

Figure 12 Comparison of NAS predictions with experimental results

The Direct Strength Method predictions for both local and distortional buckling of beams is briefly summarized here. Since the beams are fully laterally braced, the maximum capacity due to long wavelength buckling $M_{ne} = M_y$. For local buckling the capacity is:

$$\lambda_\ell \le 0.776\,,\ M_{DS\ell} = M_y \tag{1}$$

$$\lambda_\ell > 0.776\,,\ M_{DS\ell} = \left(1 - 0.15\left(\frac{M_{cr\ell}}{M_y}\right)^{0.4}\right)\left(\frac{M_{cr\ell}}{M_y}\right)^{0.4} M_y \tag{2}$$

$$\lambda_\ell = \sqrt{M_y / M_{cr\ell}} \tag{3}$$

Where $M_{cr\ell}$= critical elastic local buckling moment and M_y = moment at first yield. For distortional buckling the capacity is:

$$\lambda_d \leq 0.673,\ M_{DSd} = M_y \tag{4}$$

$$\lambda_d > 0.776,\ M_{DSd} = \left(1 - 0.22\left(\frac{M_{crd}}{M_y}\right)^{0.5}\right)\left(\frac{M_{crd}}{M_y}\right)^{0.5} M_y \tag{5}$$

$$\lambda_d = \sqrt{M_y / M_{crd}} \tag{6}$$

Where M_{crd} = Critical elastic distortional buckling moment. As shown in

Table 6, the Direct Strength Method provides good agreement with both test series. The overall agreement for M_{DSM} in the distortional buckling tests indicates that distortional buckling dominated the failure mechanism when the compression flanges were unrestrained and validates the general expression used for distortional buckling in the DSM method (which was calibrated to other data).

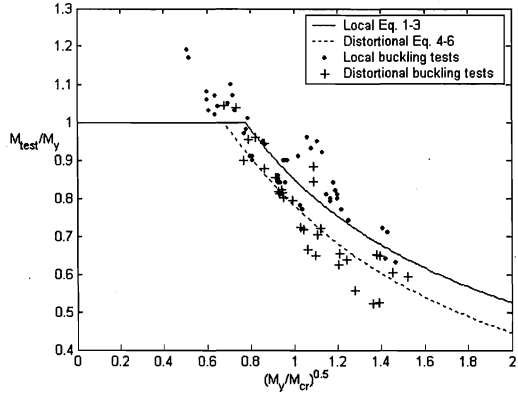

Figure 13 Direct Strength Method vs. test result

Figure 13 provides a graphical representation of Equations 1 - 6 along with the results for both the local and distortional buckling tests. In the figure M_{cr} represents $M_{cr\ell}$ for local buckling tests and M_{crd} for distortional buckling tests. It is shown that the average upper and lower bounds of laterally braced beams are well captured by the local and distortional buckling equations of the Direct Strength Method. Local buckling test data are relatively more concentrated along the corresponding design curve than that of distortional buckling tests.

The distortional buckling data show more deviation as the slenderness $(M_y/M_{cr})^{0.5}$ increases.

Finite Element Analysis

In an effort to expand the tested experimental database and to investigate the influence of moment gradient and alternate bracing conditions on Z and C beams we have initiated a nonlinear finite element study of our testing. This section reports the initial modeling selections and calibration to the Phase 1 local buckling tests reported in Yu and Schafer (2003) and the Phase 2 distortional buckling tests reported here. The calibrated finite element model will be used to extend the findings of the testing and provide specification guidelines for cold-formed steel beams used in practice.

Modeling

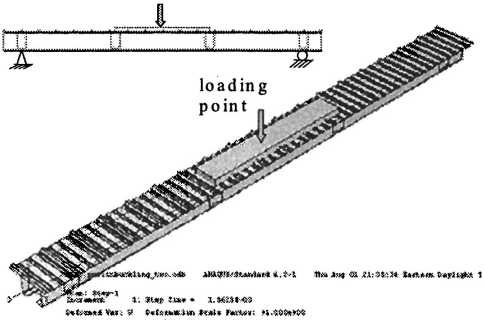

Figure 14 Finite element modeling of local buckling tests

The commercial finite element package ABAQUS 6.2 (ABAQUS 2001) is employed. An overall view of the finite element model is presented in Figure 14. Four-node linear shell elements with reduced integration are used for the purlin, panel and tubes (S4R). The loading beam uses 8-node linear solid elements (C3D8). Details of the component connections in the model are shown in Figure 15. Actual tension test results are used for the material stress-strain properties, after converting from engineering stress-strain (σ_e, ε_e) to true stress-strain (σ_t, ε_t) via the following: $\sigma_t = \sigma_e(1+\varepsilon_e)$, $\varepsilon_t = \ln(1+\varepsilon_e)$.

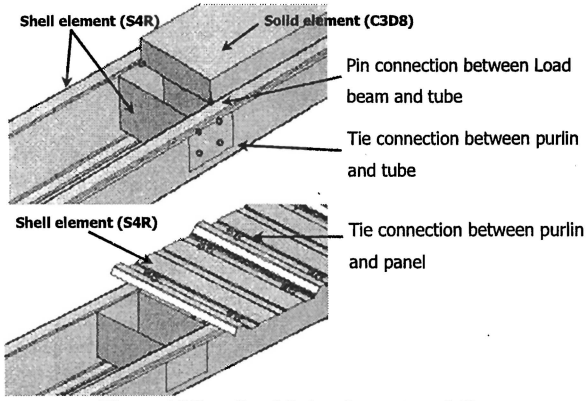

Figure 15 Details of finite element modeling

The finite element analysis is performed in a displacement control mode, consistent with the actual testing. The automatic Stabilization technique (*stabilize in ABAQUS) is adopted in the nonlinear static analysis, ABAQUS offers the option to stabilize this class of problems which involve local instabilities by applying artificial damping throughout the model in such a way that small artificial viscous forces are introduced that are sufficiently large to prevent instantaneous buckling or collapse but small enough not to affect the behavior. The arc-length based Riks method was also considered in the analysis; however, compared with the automatic Stabilization method, the latter has consistently provided better simulation of the actual tests and less convergence problems near the peak loads.

Geometric Imperfection

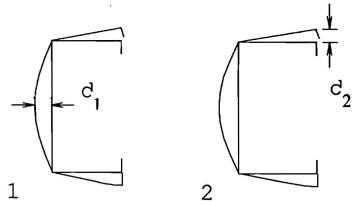

Figure 16 Definition of geometric imperfections

Geometric imperfections have a significant effect on the strength and post-buckling behavior of C and Z beams. Previous research measured geometric imperfections of cold-formed steel members, and sorted in two categories: type 1, maximum local imperfection in a stiffened element and type 2, maximum deviation from straightness for a lip stiffened or unstiffened flange as shown in Figure 16. The cumulative distribution function (CDF) values (Table 7) of the

maximum imperfection for both two types are available. A CDF value is written as $\mathbf{P}(\Delta<d)$ and indicates the probability that a randomly selected imperfection value Δ, is less than a deterministic imperfection d.

Table 7 CDF values for maximum imperfection (Schafer and Peköz 1998b)

	Type 1	Type 2
$\mathbf{P}(\Delta<d)$	d_1/t	d_2/t
0.25	0.14	0.64
0.50	0.34	0.94
0.75	0.66	1.55
0.95	1.35	3.44
0.99	3.87	4.47
mean	0.50	1.29
st. dev.	0.66	1.07

The geometric imperfections were not measured for both phases of the tests; the imperfections used in the finite element model were based on the CDF values (from Schafer and Peköz 1998b) summarized in Table 7. Knowing the amplitude of imperfections in the lowest eigenmodes is often sufficient to characterize the most influential imperfections. We conservatively assume that the type 1 imperfection may be applied to the local buckling mode and the type 2 imperfection applied to the distortional buckling mode.

Comparison with Experimental Data

For each test, two magnitudes of geometric imperfections are generated, the first uses a 25% CDF maximum magnitude, and the second a 75% CDF imperfection, thus covering the middle 50% of anticipated imperfection magnitudes. The imperfection shape is obtained by superposing the local and distortional buckling mode, scaled to the appropriate CDF value. For numerical efficiency, the finite strip analysis by CUFSM is used to generate the buckling shapes.

The finite element analysis results are summarized in Table 8 for the local buckling tests and Table 9 for the distortional buckling tests, where P_{test} is the peak actuator load, $P_{25\%}$ and $P_{75\%}$ are the peak load of the simulation with 25%, 75% CDF of maximum imperfection respectively. On average, the failure loads are bounded by the two finite element simulations with 25% and 75% CDF maximum imperfections. The pair of simulations shows that the middle 50% of imperfections exhibit a range of 14% of the bending capacity, thus providing a measure of the imperfection sensitivity. Average test-to-predicted ratios for the

finite element analysis of the local buckling tests are closer to 100% than the distortional buckling tests. The finite element analysis for the distortional buckling tests shows slightly greater scatter (greater imperfection sensitivity) and the mean response of the FE simulations is slightly greater than the average tested strength. Figure 17 shows the FEM accuracy vs. web slenderness, and indicates a slight tendency for the finite element analysis to over-predict the observed strength for very slender sections and under-predict for stockier sections. This may be partially driven by the choice of a constant d/t imperfection size – thus leading to smaller imperfection sizes for the more slender members which typically employ thinner material.

In total it is concluded that the elastic, post-buckling, and peak strength behavior of the beams are well simulated by this finite element model and its assumptions. However, the post-collapse behavior and final mechanism formation is only approximated by the model. Lack of agreement in the large deflection post-collapse range could be a function of the solution scheme (e.g., use of artificial damping via the *stabilize option) or more basic modeling assumptions, such as ignoring any plasticity in the panels. Figure 18 shows typical FE simulations for a nominal 8.5 in. deep Z beams.

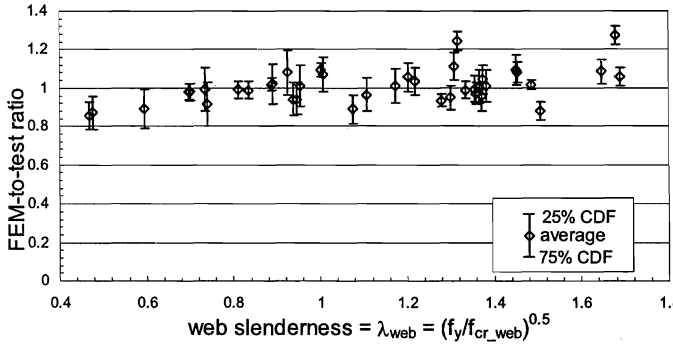

Figure 17 Comparison of finite element results with tests

Table 8 Summary of finite element analysis results for local buckling tests

	P_{test} (lbs)	$P_{25\%}$ (lbs)	$P_{25\%}/P_{test}$	$P_{75\%}$ (lbs)	$P_{75\%}/P_{test}$
8.5Z120-3E2W	17520	17968	103%	16484	94%
8.5Z105-2E1W	16720	17294	103%	15806	95%
8.5Z092-4E2W	11330	11901	105%	11170	99%
8.5Z082-1E2W	10130	11446	113%	10749	106%
8.5Z073-4E3W	8341	8770	105%	7309	88%
8.5Z065-3E1W	5969	6771	113%	5886	99%
8.5Z059-2E1W	6180	6749	109%	5748	93%
11.5Z073-2E1W	12120	13956	115%	12396	102%
11.5Z082-2E1W	17123	17294	101%	15806	92%
11.5Z092-1E2W	22000	23417	106%	19790	90%
8.5Z059-4E3W	6275	6855	109%	5763	92%
8C097-2E3W	10770	11175	104%	10200	95%
8C068-4E5W	6476	6762	104%	5614	87%
8C054-1E8W	3492	3849	110%	3233	93%
8C043-5E6W	3195	3574	112%	3082	96%
6C054-2E1W	2803	2882	103%	2240	80%
4C054-1E2W	1731	1720	99%	1365	79%
12C068-9E5W	6505	6697	103%	5968	92%
3.62C054-1E2W	1263	1170	93%	987	78%
12C068-3E4W	8542	9458	111%	8655	101%
10C068-2E1W	4381	4233	97%	3937	90%
8C068-1E2W	6141	6854	112%	5557	90%
8C043-3E1W	2985	3482	117%	3026	101%
average			106%		93%
standard deviation			6%		7%

Table 9 Summary of finite element analysis results for dist. buckling tests

	P_{test} (lbs)	$P_{25\%}$ (lbs)	$P_{25\%}/P_{test}$	$P_{75\%}$ (lbs)	$P_{75\%}/P_{test}$
D8.5Z120-4E1W	15870	16283	103%	14839	94%
D8.5Z115-1E2W	14837	16402	111%	13028	88%
D8.5Z092-3E1W	9566	10740	112%	8779	92%
D8.5Z082-4E3W	7921	9160	116%	7775	98%
D8.5Z065-7E6W	5826	6891	118%	6053	104%
D11.5Z092-3E4W	16377	16817	103%	14443	88%
D8.5Z065-4E5W	4993	5876	118%	5155	103%
D11.5Z082-4E3W	14578	15172	104%	14473	99%
D12C068-1E2W	6160	8157	132%	7566	123%
D8C043-4E2W	2678	3051	114%	2751	103%
D12C068-10E11W	5912	5497	93%	4930	83%
D8C033-1E2W	1024	1089	106%	950.8	93%
D8C054-7E6W	3032	3363	111%	2919	96%
D10C068-4E3W	3185	3235	102%	2746	86%
D8C097-5E4W	10350	12353	119%	9985	96%
D3.62C054-3E4W	1071	1027	96%	838	78%
average			110%		95%
standard deviation			8%		8%

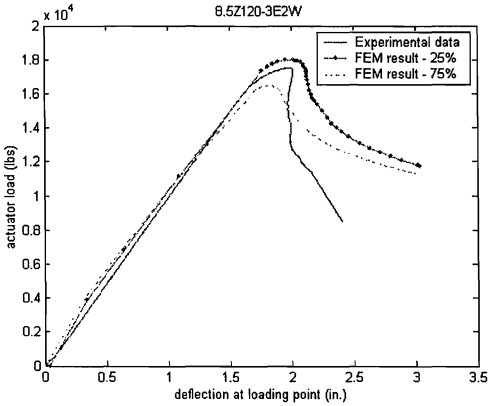

Figure 18 Comparison of test with finite element analysis results

Discussion

Experiments on a wide variety of industry standard laterally braced C and Z beams where the compression flange is unrestrained over a distance of 64 in. indicate that distortional buckling is the most likely failure mode. Distortional failures occur even when local buckling is at a lower critical elastic moment than distortional buckling. Previous testing (Phase 1 of this project) demonstrated that if additional rotational restraint can be provided to the

compression flange, such as through engagement of a through-fastened deck, the distortional mode can be avoided and a local mode triggered instead. Here, without the deck, in nearly all of the sections distortional buckling dominated the failure; though other limit states are possible, even at unbraced lengths of 64 inches. For example, in one test on an 8 in. deep C beam with a nominal t = 0.097 in. and a 64 in. unbraced length lateral-torsional buckling (LTB) initiated the failure. Identical specimens were tested with an additional midpsan connection and successfully restricted LTB. The thicker specimens have high local and distortional buckling stresses and can thus be more readily controlled by LTB. The thinnest specimens may also be controlled by other limit states, one member was observed to fail in local buckling, and another in a shear + bending failure (see the full report by Yu and Schafer 2004 for further details). While these failure modes were uncommon they serve to demonstrate the variety of behavior that may occur at even modest unbraced lengths.

The experimental data and our validated finite element model are being used to study the buckling behavior of C and Z sections with different restraint configurations. We intend to develop new design procedures for cold-formed steel beams with and without panels attached to the compression flange and to form the basis for more advanced design methods that account for partial restraint of the flange. At the same time, research is underway to explore the influence of moment gradient on the bending strength of laterally braced cold-formed steel members and development of code provisions to account for these phenomena as well.

Conclusions

Comparison of the experimental results with existing and proposed design specifications indicates that the previously employed American Specification (AISI) and Canadian Standard (S136) as well as the newly adopted North American Specification (NAS) provide a poor prediction of the strength for members failing in the distortional mode. Errors are, on average, 10 – 15 % unconservative for these design specifications. The Eurocode which provides some measures for distortional buckling is, on average, 4% unconservative. Two methods which include explicit procedures for distortional buckling the Australian/New Zealand (AS/NZS) standard and the Direct Strength Method (recently adopted as Appendix 1 of the NAS) provide far better predictions in distortional failures with conservative errors of, on average, 2% and 1% for the respective methods.

Acknowledgements

The sponsorship of AISI for both phases of this work, and MBMA for phase 1 and a graduate fellowship is gratefully acknowledged. Donation of materials by Varco-Pruden, Clark Steel and the Dietrich Design Group is also gratefully acknowledged. The assistance of the AISI task group in developing the testing plan is appreciated. Don Johnson, Maury Golovin, Joe Nunnery, Joe Wellinghoff, and Steve Thomas have all been helpful with their ideas and generous with their time. The experiments would not have been possible without the help of Johns Hopkins undergraduates, Liakos Ariston, Brent Bass, Andrew Myers, Sam Phillips, and Tim Ruth, Sam's work during Phase 1 and Tim's during Phase 2 has been particularly helpful. Finally, the work has been helpfully aided by the laboratory technician Jack Spangler, and our machinist Jim Kelly.

Appendix. - References

ABAQUS (2001). ABAQUS Version 6.2., ABAQUS, Inc. Pawtucket, RI. (www.abaqus.com)

AISI (1996). "Specification for the Design of Cold-Formed Steel Structural Members. 1996", American Iron and Steel Institute. Washington, D.C.

AS/NZS (1996). AS/NZS 4600: 1996 Cold-Formed Steel Structures. Standards Australia and the Australian Institute of Steel Construction

ASTM (2000) "E8-00, Standard test methods for tension testing of metallic material", American Society for Testing and Materials. Pennsylvania.

DSM (2003) "Appendix 1 of the North American Specification for the Design of Cold-formed Steel Structural Members." American Iron

Elhouar, S., Murray, T.M. (1985) "Adequacy of Proposed AISI Effective Width Specification Provisions for Z- and C-Purlin Design." FSEL/MBMA 85-04, Univ. of Oklahoma.

EN1993 (2002) "European Standard EN1993-1-3. Eurocode 3: Design of steel structure" European Committee for Standardization.

and Steel Institute, Washington, D.C.

Hancock, G.J., Rogers, C.A., Schuster, R.M. (1996). "Comparison of the Distortional Buckling Method for Flexural Members with Tests." *13th In'l. Spec. Conf. on Cold-Formed Steel Structures*, 125-140, St. Louis, MO.

NAS (2001). " North American Specification for the Design of Cold-Formed Steel Structural Members.", American Iron and Steel Institute, Washington, D.C.

Rogers, C.A., Schuster, R.M. (1995) "Interaction Buckling of Flange, Edge Stiffener and Web of C-Sections in Bending." Research Into Cold Formed Steel, Final Report of CSSBI/IRAP Project, Department of Civil Engineering, *University of Waterloo*, Waterloo, Ontario.

S136 (1994). "Cold-Formed Steel Structural Members" S136-94. Canadian Standards Association. Ontario, Canada.

Schafer, B.W. (2002). "Local, Distortional, and Euler Buckling in Thin-walled Columns." *J. of Struct. Eng.*, ASCE, 128(3) 289-299.

Schafer, B.W. (2001). "CUFSM 2.5: Users Manual and Tutorials" (www.ce.jhu.edu/bschafer/cufsm).

Schafer, B.W., Peköz, T. (1999). "Laterally Braced Cold-Formed Steel Flexural Members with Edge Stiffened Flanges.", *J. of Struct. Eng.* ASCE, 125(2) 118-127.

Schafer, B.W., Peköz, T. (1998a). "Direct Strength Prediction of Cold-Formed Steel Members using Numerical Elastic Buckling Solutions." *14th Int'l. Spec. Conf. on Cold-Formed Steel Structures*, St. Louis, Missouri.

Schafer, B.W., Peköz, T. (1998b). "Computational Modeling of Cold-Formed Steel: Characterizing Geometric Imperfections and Residual Stresses." Elsevier, *Journal of Constructional Steel Research.* 47 (3) 193-210.

Yu, C., Schafer, B.W. (2004). "Distortional Buckling of Z and C Members in Bending." Report submitted to the American Iron and Steel Institute, Washington, D.C.

Yu, C., Schafer, B.W. (2003). "Local buckling Test on Cold-Formed Steel Beams" ASCE *Journal of Structural Engineering.* 129 (12) 1596-1606.

Appendix. - Notation

b_c	out-to-out compression flange width
b_t	out-to-out tension flange width
d_c	out-to-out compression flange lip stiffener length
d_t	out-to-out compression flange lip stiffener length
E	modulus of elasticity
f_y	yield stress
f_u	ultimate stress
h	out-to-out web depth
r_{hc}	outer radius between web and compression flange
r_{dc}	outer radius between compression flange and lip
r_{ht}	outer radius between web and tension flange
r_{dt}	outer radius between tension flange and lip
t	base metal thickness

θ_c compression flange stiffener angle from horizontal
θ_t tension flange stiffener angle from horizontal